Sixth International Conference on Durability of Concrete Structures **Paper Number ICC09**
18 - 20 July 2018
University of Leeds, Leeds, West Yorkshire, LS2 9JT, United Kingdom

Comparison of lithomarge and cement-based mortars performance in aggressive aqueous environments

J. Kwasny, T.A. Aiken, M.N. Soutsos and D.J. Cleland
School of Natural and Built Environment, Queen's University Belfast, Northern Ireland, UK

J.A. McIntosh
banah UK Ltd, Coleraine, Northern Ireland, UK

ABSTRACT

The resistance of room temperature cured geopolymer mortar (GPM) against chemical attacks, i.e. sodium and magnesium sulfate solutions, and sulfuric and hydrochloric acid solutions, was evaluated. GPM was formulated using a lithomarge precursor (low-purity kaolin) to achieve 28-day characteristic compressive strength of 60 MPa. Its performance was compared with an equivalent Portland cement mortar (PCM) having the same paste volume and strength grade. 28-day old bar samples were stored in 0.352 mol/L sulfate solutions for 52 weeks whereas 28-day old cube samples were exposed for 8 weeks to acid solutions with concentration of 0.52 mol/L. GPM showed superior performance against sulfate attack when compared to PCM. No visual deterioration was observed in GPM, the length changes were relatively small, and no changes to the microstructure were detected – in contrast to severely deteriorated PCM. As confirmed by visual observations and lower mass loss, GPM showed better resistance to attack by both acids than PCM. GPM provided a better quality (lower permeability) of an acid-degraded layer, lowering the degree of further deterioration. The main mechanisms of the matrix deterioration of GPM in both acids was dealumination of the hardened binder, with a higher degree of changes detected for sulfuric acid.

Keywords: Lithomarge; Geopolymer mortars; Portland cement mortars; Sulfate attack, Acid attack.

1.0 INTRODUCTION

Structures made with Portland cement concrete often are exposed to aggressive aqueous media. Contact of highly alkaline hardened cement paste (hcp) with water carrying aggressive ions can cause chemical and physical degradation (Mehta and Monteiro, 2006). Three main types of chemical degradation mechanisms are: an ion exchange reaction between aggressive medium and the hcp, reaction leading to leaching of ions from the hcp, and reaction causing growth of expansive products within the pore structure of hcp. These processes often occur together and lead to physical changes to the hcp microstructure: altering porosity, permeability and integrity of the concrete. Two common types of chemical attack are external sulfate attack and acid attack (RILEM TC 211-PAE, 2013).

Portland cement based materials have typically low resistance to the actions of sulfate and acid attack, which reduces the service life of the exposed structure. This results in financial, social and environmental implications associated with costly maintenance or replacement of the damaged structure. The problem of chemical attack may be addressed by applying layers of sealants or coatings on the concrete surface, or creating a physical barrier between concrete and the aggressive environment *via* protective overlays (Aguiar *et al.*, 2008). Whilst effective, these solutions proved to be costly and labour intensive. An alternative approach is to improve the performance of concrete by modifying its composition; however, such solutions vary in effectiveness. Typically, to improve sulfate resistance of concrete, either cements with reduced C_3A content are used (sulfate resistant cements) or reduced calcium hydroxide (CH) content and permeability of hcp are sought after, for instance by using blended cements (RILEM TC 211, 2013). The resistance of cement-based materials to acid attack strongly depends on the content and type of calcium rich hydration products, intrinsic permeability of undamaged concrete and most importantly – on the permeability of the acid-degraded layer (Beddoe and Dorner, 2005). Use of blended cements, partial replacement of Portland cement with additions or use of polymer modified cements was investigated to achieve above properties, however conflicting reports on their effectiveness were reported (Monteny *et al.*, 2003; Oueslati and Duchesne, 2012). A promising solution has emerged recently in the form of geopolymer binders which have been reported to have improved resistance to both these sulfate and acid attack due to their ceramic-like microstructure (RILEM TC 224-AAM, 2014; Pacheco-Torgal *et al.*, 2015).

Geopolymers are a low-carbon alternative to Portland cement-based binders in concrete. They typically consist of a powder precursor, primarily composed of amorphous alumino-silicates, and a liquid chemical activator containing an alkali source. Chemical activator provides elevated pH, in the form of hydroxides, silicates, or their blends (RILEM TC 224-AAM, 2014). When mixed, the two components undergo a dissolution/condensation reaction to form a ceramic-like amorphous microstructure (RILEM TC 224-AAM, 2014).

A wide range of potential precursors and activators may be used to produce geopolymers of varying quality (BSI, 2016). In terms of the precursor, the most common candidates are high purity kaolin and different types of clays, or waste/by-product materials, such as slags and ashes (RILEM TC 224-AAM, 2014). However, some of these materials may not be readily available across the globe or are too expensive. It is well known that in the UK and Europe, the supply of good quality fly ash for concrete applications is limited (Heath *et al.*, 2013) and will become more so due to the move away from fossil fuels for electricity generation. While almost all of the UK produced slag is used in cement production, a continuous demand of fly ash for use in blended cements or as partial replacement of Portland cement will cause increased pressure on its supplies (Heath *et al.*, 2013). Heath *et al.* (2013) anticipated that current global production of fly ash and slag cement meets only 20% of PC demand and will most likely fall below 10% by 2050. It is estimated that, despite being limited, the UK has larger resources of kaolin than fly ash (Heath *et al.*, 2013). However, high costs involved in the production of high purity metakaolin (made from clays containing at least 85% kaolin), render it uneconomical for use in the majority of geopolymer concrete applications. Consequently, locally available clays with lower kaolin content are of interest. Some of them have already been reported to produce geopolymer binders with compressive strength >50 MPa upon calcination (Arellano-Aguilar *et al.*, 2014. McIntosh *et al.*, 2014, McIntosh *et al.*, 2015, Kwasny *et al*. 2016). In Northern Ireland, a large deposit of metamorphose lateritic lithomarge forms a part of the Interbasaltic Formation (IBF) (Eyles, 1950). Lithomarge is a soft rock, primarily containing kaolinite ($Al_2Si_2O_5(OH)_4$), gibbsite ($Al(OH)_3$), goethite ($FeO(OH)$), hematite (Fe_2O_3) and various smectite minerals (McIntosh *et al.*, 2014). Geopolymer binders with strength >50 MPa were successfully formulated with calcined lithomarge obtained from rocks containing at least 60% w/w of kaolinite (McIntosh *et al.*, 2015).

2.0 RESEARCH SIGNIFICANCE

Sulfate and acid attack on clay based geopolymer binder systems has previously been investigated using geopolymers formulated with pure metakaolin (Pacheco-Torgal *et al.*, 2015). In order to encourage the use of less expensive kaolin geopolymer binders, this research aimed to assess and directly compare the resistance of lithomarge-based geopolymer and neat Portland cement mortars to chemical attack by sulfate (Na_2SO_4 and $MgSO_4$) and mineral acid (H_2SO_4 and HCl) solutions.

3.0 EXPERIMENTAL PROGRAMME

3.1 Methodology

To allow for a like-for-like comparison, one geopolymer mortar (GPM) and one Portland cement mortar (PCM) mix was selected from work reported elsewhere (Kwasny *et al.*, 2016). Mortars with both binders were optimised to have equivalent paste volumes of 500 L/m^3 and characteristic 28-day compressive strengths of 60 MPa.

In order to determine resistance of mixes to sulfate attack, 28-day old bar samples were stored in 0.352 mol/L solutions of sodium sulfate (Na_2SO_4) or magnesium sulfate ($MgSO_4$) for 52 weeks. To assess the degree of sulfate attack the visual appearance and length change were tested periodically. After 56 weeks samples exposed to sulfate solutions and those unexposed (stored in water) were tested using X-ray diffraction (XRD) and FTIR spectroscopy to determine the microstructural changes.

Resistance to acid attack was determined by immersing 28-day old cube samples in 0.52 mol/L solutions of either sulfuric acid (H_2SO_4) or hydrochloric acid (HCl) for 8 weeks. Samples were tested weekly for visual appearance and mass change. Microstructural changes were evaluated using both XRD and FTIR spectroscopy. Samples exposed to acid solutions were compared with unexposed (control) samples stored in water.

3.2 Materials

The geopolymer binder used was a two component system produced by banah UK Ltd, the powder component (here called litho750) and the liquid component (here called chemical activator). The litho750 product comprised an aluminosilicate precursor manufactured by calcination at 750 °C and subsequent grinding of the altered basalt (lithomarge), sourced from the IBF of the Antrim Lava Group in Northern Ireland (McIntosh *et al.*, 2014). Portland cement (PC) CEM I 42.5N produced in Northern Ireland and conforming to the requirements of BS EN 197-1 (BSI, 2011) was used. Chemical compositions (determined using X-ray fluorescence spectrometry) and crystal structure (determined with X-ray powder diffraction spectrometry) of litho750 and PC are given in Table 1 and Fig. 1, respectively. The main peaks in the XRD pattern of litho750 are due to hematite (H), which is present as a result of calcination of goethite and magnetite in the original kaolinite clay (McIntosh *et al.*, 2014). Crystalline

phases including alite (AE), belite (BE), aluminate (AL), brownmillerite (BR) and gypsum (G) are present in PC.

Table 1. Oxide composition and physical properties of litho750 and PC

Oxide composition [%]	Litho750	PC
SiO_2	32.04	20.21
Al_2O_3	24.99	4.79
Fe_2O_3	25.21	2.78
CaO	7.78	63.01
MgO	1.71	1.93
MnO	0.37	0.08
TiO_2	3.17	0.27
Na_2O	0.36	0.19
K_2O	0.15	0.59
SO_3	0.22	2.60
P_2O_5	0.14	0.12
LOI [%]	3.08	3.16
Specific gravity	2.89	3.13

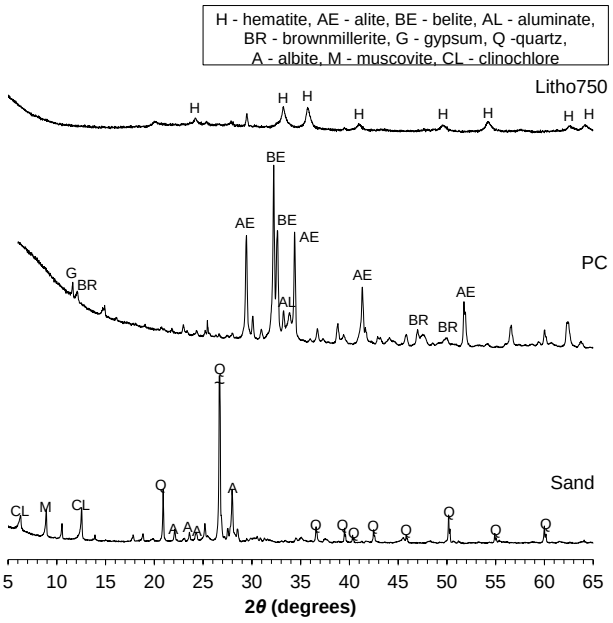

Fig. 1. XRD patterns of litho750, PC and sand

A proprietary chemical activator was an aqueous solution of alkali silicate with a water content of 41.2% and specific gravity of 1.57. Water from the mains supply (17 ±1 °C) was used as the mixing water.

Sand, with oven-dry particle density of 2695 kg/m^3, was sourced from Brackagh Quarry (Draperstown, Northern Ireland). Water absorption of sand was 0.92% at 1-hour and 1.1% at 24-hours. Density and water absorption were determined according to BS 812-2 (BSI, 1995). As shown in Fig. 1, sand was rich in quartz (Q) and also contained albite (A), muscovite (M) and clinochlore (CL).

Laboratory reagent grade chemicals, *i.e.* anhydrous Na_2SO_4, anhydrous $MgSO_4$, concentrated H_2SO_4 (95-97%) and concentrated HCl (≥37%), were used to prepare testing sulfate and acid solutions by mixing in various proportions with distilled water.

3.3 Mortar proportions

The mix proportions and the mean 28-day compressive strengths of GPM and PCM mixes are shown in Table 2. These mixes were selected from the range of mixes reported by Kwasny *et al.* (2016) and were designed following the absolute volume method.

Table 2. Mix proportions and 28-day compressive strengths of GPM and PCM mixes

	Mix ID	GPM	PCM
Material quantity [kg/m^3]	Litho750	559	-
	Chemical activator	396	-
	PC	-	676
	Sand	1347	1347
	Absorption water	12.4	12.4
	Total added water	67	296
	Free water	218	284
w/s ratio* or w/c ratio**		0.275*	0.42**
The mean compressive strength at 28-day [MPa]		77.0	77.4

3.4 Mix preparation

Mortars were prepared in a 10 L capacity planar-action high-shear mixer, in 6 L batches. Oven-dried sand was placed in a mixing bowl with half of the total water (free + absorption water) and mixed for approximately 1 minute. The sand and water mixture was then left in the mixing bowl for 15 minutes. Then litho750 (for GPM) or PC (for PCM), was introduced into the mixing bowl followed by 1 minute of mixing at low speed. The remaining half of the total water and, in the case of GPMs, the chemical activator, were added to the mixing bowl and mixed for 2 minutes at low speed. The mixer was stopped for 1 minute to crush any lumps of remaining solids. Afterwards, mixing resumed for 2 minutes at a high speed, followed by 1 minute at a low speed.

3.5 Sample casting, demoulding and conditioning

The following mortar samples were cast for each mix: six 25×25×285 mm bars and ten 50×50×50 mm cubes. Samples were cast in two layers, with each layer compacted on a vibrating table. Afterwards, they were wrapped with cling film to prevent water evaporation and placed in the conditioning room (RH >95% and 20 ±1 °C). Samples were demoulded at 24 ±0.5 hours after casting, and placed in curing containers on 15 mm height spacers. The curing containers were filled with water to the height of 5 mm, then covered with tightly fitting lids and stored in the conditioning room (20 ±1 °C). This procedure

allowed the conditioning of the samples at RH of >95% and prevented unintentional carbonation of the samples, and leaching of alkalis. After 21 days of curing, the samples were transferred to a water bath (20 ±1 °C) until 28-day, in order to ensure full water saturation before starting sulfate and acid testing. At 28-day, two control (unexposed) cube samples were left in the water bath for further testing. Separate water baths were used for each mix in order to avoid cross contamination due to leaching.

3.6 Testing procedures

Resistance to sulfate attack was tested in similar way to the procedure described in ASTM C1012 (ASTM, 2004) by measuring the length change of mortar samples immersed in sulfate solutions. The samples were 25×25×285 mm mortar bars equipped with 6 mm diameter stainless steel balls at each end. The length of the bars was measured initially at 28-day after casting, and then sets of three bars from each mix were placed vertically in airtight plastic storage containers filled with 0.352 moles of Na_2SO_4 or $MgSO_4$ per litre of solutions (equivalent to 5% and 4.24% concentrations, respectively). The proportion of sulfate solution volume to samples volume in a storage container was kept at approximately 4.4 (*i.e.* 800 mL of solution per mortar bar). Samples were kept in the sulfate solutions (20 ±1 °C) for a total of 52 weeks, during which their length was measured at specific intervals (every week for the duration of the first 4 weeks, then every two weeks for the duration of 8 weeks, and 4 weeks for the remaining 40 weeks). Before the length measurement was determined, samples were visually inspected and their surface was gently dried by hand with a moist paper towel to achieve saturated and surface-dry condition. During the first 12 weeks of testing, sulfate solutions were renewed every 2 weeks, and every 4 weeks afterwards. The length change, expressed in microstrain, was calculated for the nominal gauge length of 280 mm (inner distance between stainless steel balls) and is reported as an average of three measurements. After 52 weeks of testing, samples were collected from the outermost surface layer of the mortar bars exposed to sulfate solution (no deeper than 0.5 mm) and from the middle of the fractured control cube sample kept in water bath. These samples were transferred to airtight bottles and then further processed before XRD and FTIR analysis.

Resistance to H_2SO_4 and HCl acid attack was determined using an accelerated method, based on the general guidelines provided in ASTM C267 (ASTM, 2001). Mass loss of mortar samples, *i.e.* 50 mm size cubes, immersed in acid solution, was investigated. At 28-day the mass of each cube was measured and sets of four cubes from each mix were placed in plastic boxes containing acid solutions (20 ±1 °C) with concentrations of 0.52 moles of H_2SO_4 (*i.e.* 5%) or HCl (*i.e.* 1.86%) per litre of solution. The volume proportion of acid solution to samples in a storage container was approximately 0.9. Every 7 days, any loose material was removed from each sample by gentle brushing under a stream of tap water. Then, surface of each sample was gently dried by hand with a moist paper towel to achieve saturated and surface-dry condition. Visual inspection was subsequently carried out and the mass of each cube was recorded. Before disposing, the used acid solutions were filtered to collect the debris material remaining in the storage boxes. Cubes were returned to the boxes and then boxes were filled with fresh acid solutions. This procedure was repeated for 8 consecutive weeks. An average cumulative mass loss is reported. Collected debris material from storage boxes, and that from the middle of the fractured control cube sample kept in water bath, were placed in airtight bottles for further processing prior to XRD and FTIR examination.

After collection, samples for XRD and FTIR spectroscopy studies were transferred to a desiccator and stored for *ca.* 24 hours under vacuum at 40 ±1 °C to evaporate the moisture. Then, dried samples were powdered using mortar and pestle to pass a 63 µm sieve. Immediately after grinding, the powdered samples were placed in sealable plastic bags and stored in the desiccator under vacuum at 20 ±1 °C until testing.

Powdered samples were analyzed using XRD, with a PANalytical X'Pert PRO diffractometer, to identify the crystalline components and observe potential changes caused by either sulfate or acid attack. Diffraction patterns were collected between 5° and 65° 2θ with a step size of 0.016°. PANalytical X'Pert Highscore software with the Powder Diffraction File database was used to identify the mineralogy of the samples based on the diffraction patterns.

To qualitatively identify bond degradation due to sulfate and acid attack, powdered samples were analyzed using FTIR spectroscopy. A Jasco 4100 series FTIR Spectrometer with Attenuated Total Reflectance attachment (germanium crystal) was used. The spectra were recorded between 650 and 4000 cm^{-1}.

4.0 RESULTS AND DISCUSSION

The effect of sulfate attack on physical and microstructural features of geopolymer and Portland cement mortars is discussed first and is followed by discussion of the effect of acid attack on these mortars.

4.1 Resistance to sulfate attack

The resistance of PCM and GPM samples to sulfate attack is presented in this section. Description of the visual appearance and length changes of samples is followed by microstructural changes determined by XRD analysis and FTIR spectroscopy.

Visual appearance

The visual appearance of samples after 52 weeks of exposure to solutions of 0.352 mol/L of Na_2SO_4 and $MgSO_4$ are shown in Fig. 2.

Fig. 2. Visual appearance of GPM and PCM samples after 52 weeks of exposure to 0.352 mol/L solutions of a) Na_2SO_4 and b) $MgSO_4$

There was no sign of discoloration, expansion or cracking on the surface of any of the GPM samples. In contrast, PCM samples showed variable degree of deterioration. Surfaces of PCM samples stored in Na_2SO_4 solutions were covered with a net of microcracks (Fig. 2a). The samples were curled, broken, and longitudal and lateral expansion was easily noticeable. Surfaces of PCM samples exposed to $MgSO_4$ solution were coated with a layer of white precipitates (Fig. 2b), which has been confirmed as magnesium sulfate hydrate (section on XRD). Edges of PCM samples became rounded, due to loss of degraded material. Although PCM samples showed visible expansion, they maintained their initial shape.

Length change

The length change of mortar bar samples exposed to the sulfate solutions are shown in Fig. 3.

Samples of GPM proved to be stable in sulfate solutions, exhibiting relatively small change in length. GPM bars exposed to Na_2SO_4 showed minor shrinkage of less than 300 microstrain, while samples stored in $MgSO_4$ solution showed minor expansion not exceeding 100 microstrain. It is not clear what caused the shrinkage of the samples stored in Na_2SO_4.

As expected, PCM samples exposed to sulfate ions showed considerably larger expansion than GPM samples. This was due to transport of sulfate ions into hcp pore structure and then reaction with hcp to form expansive salts (Aye and Oguchi, 2011). At the same age, PCM samples exposed to Na_2SO_4 had larger expansion than those stored in $MgSO_4$ solution (at 52 week the expansion reached nearly 4300 and 3900 microstrain, respectively). This was linked to the type of expansive salts formed, and is discussed in the section on XRD. For all PCM, expansion occurred in two stages, where 'induction' period characterized by low expansion value was followed by steady increase in expansion (Santhanam *et al.*, 2002). For Na_2SO_4 attack the transition between these two stages occurred earlier and was sharper (Santhanam *et al.*, 2002).

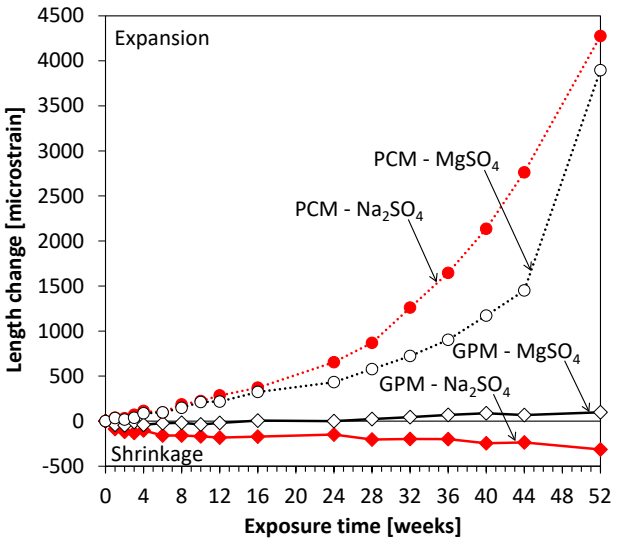

Fig. 3. Length change of GPM and PCM exposed to Na_2SO_4 and $MgSO_4$ solutions

XRD

Fig. 4 shows the XRD spectra for the material collected from the outermost surface layer of GPM and PCM, which were subjected to attack by Na_2SO_4 and $MgSO_4$ solutions. The spectra obtained from the center of the samples unexposed to sulfate attack (stored in water) are shown for comparison.

The main crystalline phase present in the unexposed GPM sample was hematite (H) with the main peaks observed at 2θ of 24.1, 33.2, 35.6 and 54.1°. In the unexposed PCM, calcium hydroxide (CH) was identified by peaks at 2θ of 18.1, 28.7, 34.1, 47.1 and 50.8°. Both mortars contain quartz (Q), albite (AB), muscovite (M) and clinochlore (CL) due to the presence of sand (XRD pattern of sand is shown in Fig. 1). The main quartz peaks are observed at 2θ of 20.9, 26.7, 36.6, 39.5, 42.5, 50.2 and 60.0°. The peaks at 2θ of 28.0 and 8.8° correspond to albite and muscovite, respectively. Finally, the peaks due to clinochlore are observed at 2θ of 6.3 and 12.5°.

After 52 weeks of either Na_2SO_4 or $MgSO_4$ attack, XRD patterns of the GPM samples showed no significant change when compared with unexposed samples, proving the stability of the geopolymer mixes in sulfate environments.

For the PCM samples, major changes to XRD patterns were observed. CH was not present after exposure to both Na_2SO_4 and $MgSO_4$ solutions, which suggests its dissolution. Exposure of PCM to Na_2SO_4 caused the formation of ettringite (E) and gypsum (G). Ettringite was observed by peaks at 2θ

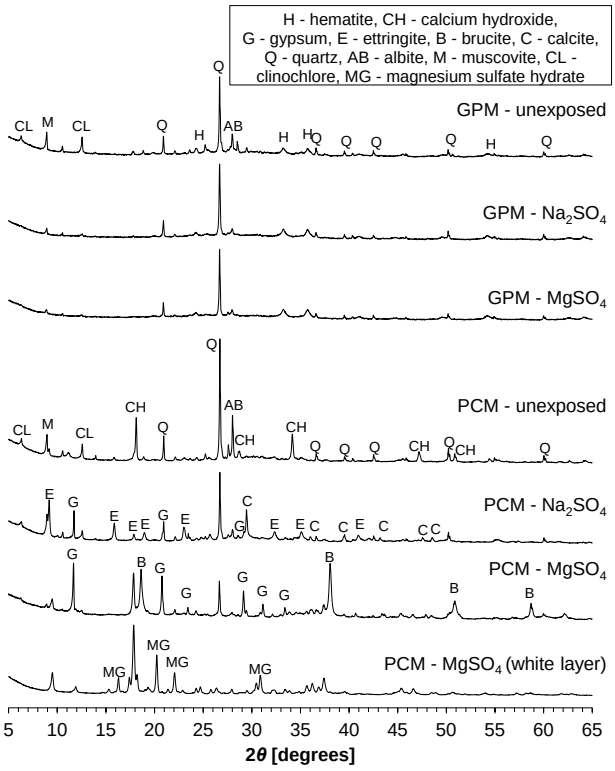

Fig. 4. XRD patters of unexposed GPM and PCM samples and samples exposed for 52 weeks to Na_2SO_4 and $MgSO_4$ solutions

of 9.1, 15.8, 17.8, 18.9, 22.9, 32.4, 35.0 and 40.9°. The peaks at 2θ of 11.7, 20.7 and 29.2 are attributed to gypsum. Also calcite (C) was observed in the sample exposed to Na_2SO_4 by peaks at 2θ of 29.4, 36.0, 39.4, 43.2, 47.5 and 48.5°. Exposure to $MgSO_4$ resulted in the formation of an increased amount of gypsum highlighted by peaks at 2θ of 11.7, 20.7, 23.4, 29.2, 31.1, and 33.4°. Magnesium hydroxide, *i.e.* brucite (B), also formed, and resulted in peaks at 2θ of 18.6, 38.1, 50.9 and 58.7°. Since ettringite is not stable below a pH of approximately 10.6, it was not detected in samples exposed to $MgSO_4$, but was present in samples exposed to Na_2SO_4. The above results for PCM exposed to both sulfate solutions are in good agreement with the literature (Aye and Oguchi, 2011). It is well known that ettringite occupies larger volume than gypsum (Monteny *et al.*, 2000). As ettringite was predominantly detected in samples exposed to Na_2SO_4, this explained their larger length change discussed in previous section. In addition, lower expansion of PCM exposed to $MgSO_4$ may be attributed to the precipitation of brucite in the outmost surface layer of samples, which temporarily restricted penetration of Mg^{2+} into the pore structure (Bonen and Cohen, 1992). As shown in Fig. 2, a white precipitate formed on the outside of the PCM exposed to $MgSO_4$. This precipitate was carefully collected and processed for XRD analysis as other samples. It was established that this layer mainly consisted of magnesium sulfate hydrate (MG) with peaks at 2θ of 16.3, 20.2, 22.0, 30.4 and 30.8°.

FTIR spectroscopy

Figure 5 shows the FTIR spectra for the outermost surface layer of GPM and PCM samples exposed to Na_2SO_4 and $MgSO_4$ solutions. They are compared to the spectra of inner section of the control (unexposed) samples, which were stored in water.

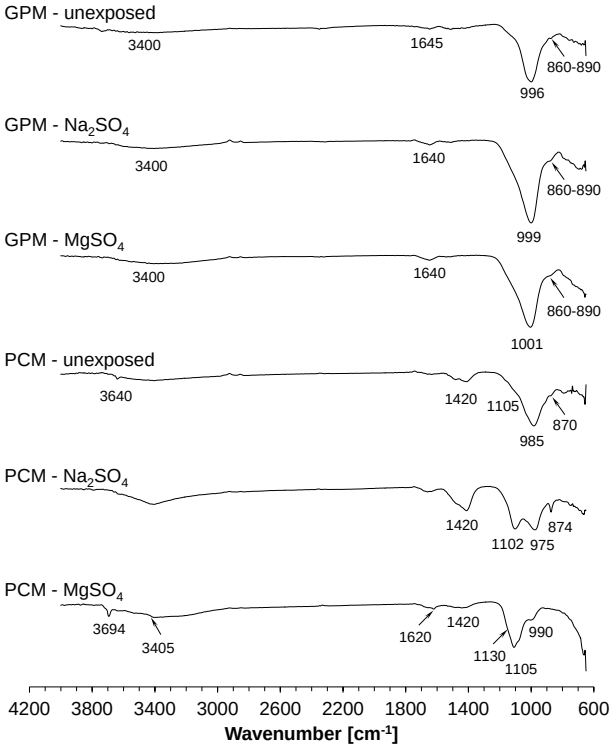

Fig. 5. FTIR spectra of unexposed GPM and PCM samples and samples exposed for 52 weeks to Na_2SO_4 and $MgSO_4$ solutions

The unexposed sample of GPM had a characteristic sharp band located at approximately 996 cm^{-1}, assigned to asymmetric T-O stretching (T = Si or Al), and a shoulder at approximately 860–890 cm^{-1}, related to M-O vibrations (M = K) (Gao *et al.*, 2013). The peak at approximately 1640 cm^{-1} and broad band centered at approximately 3400 cm^{-1} can be assigned to bending and stretching vibrations of water, respectively (Gao *et al.*, 2013). After the exposure of geopolymer samples to either of the sulphate solutions, there was very little change in the spectra, except for the main band located at around 996 cm^{-1}, which increased its intensity, but did not change the position.

In the case of both PCMs, intensity of a band observed in unexposed sample at 985 cm^{-1}, attributed to asymmetric Si-O stretching vibrations in C-S-H, reduced when samples were exposed to sulphate solutions (Ghosh, 1999). A band at 3640 cm^{-1}, corresponding to O-H stretching vibrations in CH was not present in both samples exposed to sulfate solutions. The intensity of a broad shoulder near 1105 cm^{-1}, corresponding to asymmetric stretching vibrations of SO_4^{2-} in ettringite, became higher for

samples stored in sulfate solutions (Ghosh, 1999). Presence of gypsum was detected in $MgSO_4$ sample, (shoulder at 1130 cm^{-1}, weak peak at 1620 cm^{-1} due to in plane bending vibrations of O-H···O group, and weak peak at 3405 cm^{-1} due to stretching vibrations of O-H (Putnis *et al.*, 1990). Presence of brucite ($Mg(OH)_2$) in a sample exposed to $MgSO_4$ solution was confirmed by a strong O-H vibration at 3694 cm^{-1}. For samples exposed to Na_2SO_4 higher intensity of $CaCO_3$ was observed at wavenumber 874 cm^{-1} (out of plane bending of CO_3^{2-}), and broad band centered around 1412 cm^{-1} (asymmetric stretching of CO_3^{2-}).

4.2 Resistance to acid attack

The resistance of PCM and GPM samples to acid attack of H_2SO_4 and HCl solutions is presented in this section. Description of the visual appearance and mass changes of samples is followed by microstructural changes determined by XRD analysis and FTIR spectroscopy.

Visual appearance

The visual appearance of samples after 8 weeks of exposure to 0.52 mol/L solutions of H_2SO_4 and HCl acids are shown in Fig 6.

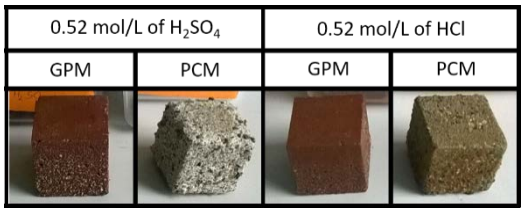

Fig. 6. Visual appearance of GPM and PCM after 8 weeks of exposure to H_2SO_4 and HCl acid solutions

Regardless of the acid type, GPM samples showed less surface deterioration than the PCM samples. In general, GPM and PCM samples exposed to H_2SO_4 solution deteriorated more than those attacked by HCl solution. The acid type did not have a significant effect on the edge deterioration of GPM samples. For PCM mixes, the edges of samples exposed to H_2SO_4 solutions became rounded, while they were relatively well preserved in HCl solutions. Neither of the two acids resulted in a colour change of the GPM samples. PCM samples exposed to H_2SO_4 acid solutions had white precipitation on the surface, while the surface of samples stored in the HCl solutions turned light brown in parts. The white precipitation was identified as gypsum (as discussed in the XRD section). The light brown discoloration is likely related to precipitation of loosely bound ferric hydrates at pH above 2 (Gutberlet *et al.*, 2015).

Mass change

Mass changes in mortar samples during 8 weeks of immersion in 0.52 mol/L H_2SO_4 and HCl solutions are shown in Fig. 7.

The rate of mass loss in GPM samples exposed to H_2SO_4 was decreasing from one cycle to the next during the 8 weeks of the test. For PCM samples the mass loss rate increased initially and after week 2 it was stabilised at an approximately constant rate. GPM reached mass loss of 7.7% at week 8 while for PCM 24.9% mass loss was recorded. The high mass loss of PCM was the result of a high degree of hcp decalcification and, most importantly, the result of progressive degradation of the surface layer caused by pressure exerted by expansive crystals of the salts formed (XRD results confirmed the presence of gypsum) inside the pore structure (Monteny *et al.*, 2000). A layer-by-layer degradation of the sample surface caused by the expansive spalling offset the increase in mass associated with salts formation (Gutberlet *et al.*, 2015).

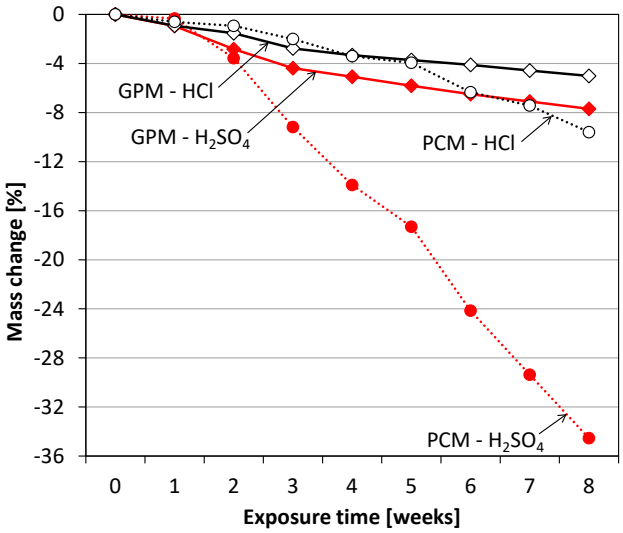

Fig. 7. Mass loss of GPM and PCM exposed to H_2SO_4 and HCl solutions

When exposed to HCl solutions, the rate of mass loss of the GPM mixes during the 8 weeks of the test was decreasing from one cycle to the next. At the end of the test the mass loss observed for mix GPM was 5.0%. The rate of mass loss of PCM samples exposed to HCl solutions was increasing from one cycle to the next, due to decalcification of the samples and, to a lesser extent, to release of aluminium and iron (Gutberlet *et al.*, 2015). At the end of the test, the PCM mass loss was 9.6%.

Irrespective of the acid type, it appears that for GPM mixes the mass loss rate decreased during the course of the test (and stabilised somewhere between the third and the fifth week of the test), while for PCM it accelerated. This suggests that the degraded layer of the material in GPM mixes acted as a buffer zone and slowed down further progression of the acid attack, thus providing better overall resistance against the acid attack than the PCM counterparts.

Where acid type is concerned, GPM and PCM exposed H_2SO_4 solutions lost relatively more mass than comparable mixes stored in HCl solutions.

XRD

The XRD patterns of the materials collected from the center of unexposed GPM and PCM samples are compared in Fig. 8 with the XRD patterns recorded for the degraded layer, collected from samples exposed for 8 weeks to H_2SO_4 and HCl solutions. The unexposed samples used in acid attack testing (Fig. 8) have very similar XRD patterns to the unexposed samples used for sulfate attack (Fig. 4), hence, the discussion of these XRD results is not repeated here.

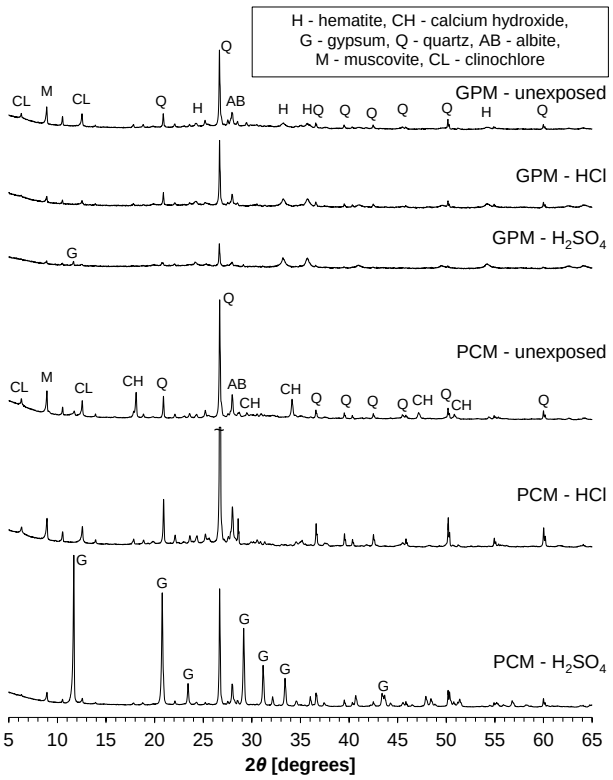

Fig. 8. XRD patterns of unexposed GPM and PCM samples and samples exposed for 8 weeks to HCl and H_2SO_4 solutions

Very little change upon the acid attack was observed in GPM, particularly for HCl acid attack, which is in agreement with results reported by Bouguermouh *et al.* (2017). for metakaolin based geopolymers. Following the H_2SO_4 attack, a small peak corresponding to gypsum was identified at 2θ of 11.7° in the XRD pattern, revealing that calcium in the calcined lithomarge reacted with H_2SO_4 to form gypsum.

The XRD patterns of the PCM showed greater changes after acid attack. CH was no longer identified after attack by either HCl or H_2SO_4, suggesting it had reacted with the respective acid. After H_2SO_4 attack, gypsum was identified by peaks at 2θ of 11.7, 20.7, 23.4, 29.2, 31.1, 33.4 and 43.3°.

FTIR spectroscopy

Fig. 9 shows the FTIR spectra of the material deteriorated from GPM and PCM samples subjected to acid attack in 0.52 mol/L solutions of H_2SO_4 or HCl. The spectra obtained from the centre of unexposed samples are shown for the comparison.

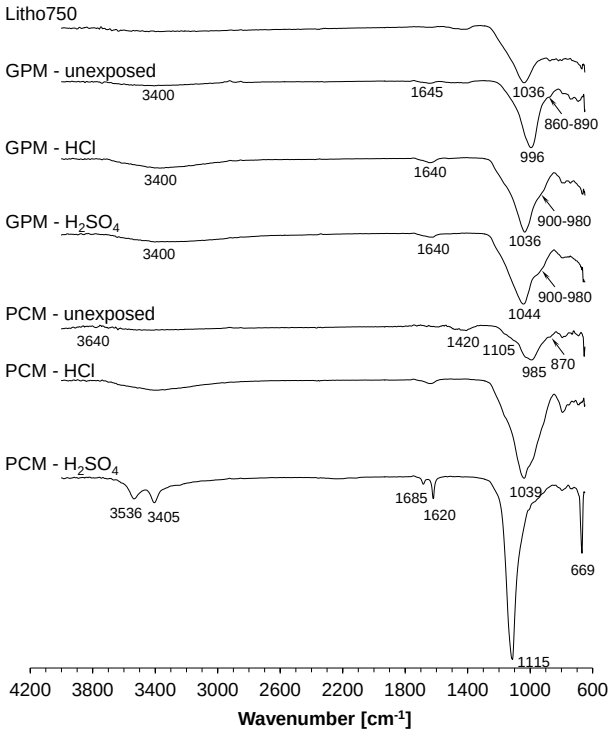

Fig. 9. FTIR spectra of unexposed GPM and PCM samples and samples exposed for 8 weeks to HCl and H_2SO_4 solutions

For the unexposed geopolymer sample the main peak was at 996 cm^{-1} (asymmetrical T-O vibrations, where T = Si or Al (Gao *et al.*, 2013)). It shifted to 1036 and 1044 cm^{-1} after HCl and H_2SO_4 acid attacks, respectively, suggesting that acid attack caused an increase in the Si/Al ratio due to the removal of aluminium from the binder (Burciaga-Díaz and Escalante-García, 2012). Bernal *et al.* (2012) reported that the extent of the shift to higher wavenumbers can be related to the degree of structural damage to the binder. In this case, H_2SO_4 acid caused a larger shift of the peak and also caused a larger mass loss than HCl (Fig. 7). Of notice is that the FTIR spectrum for the unreacted litho750 featured a strong signal at 1036 cm^{-1}, similarly to acid attacked samples. It suggests that, in addition to the degraded (dealuminated) binder and sand, the corroded samples contained unreacted calcined lithomarge particles (Burciaga-Díaz and Escalante-García, 2012). A shoulder at 900–980 cm^{-1} appeared for samples attacked by either acid, which can be attributed to the removal of K^+ ions and the incorporation of H_3O^+ ions in the degraded structure (Burciaga-Díaz and Escalante-García, 2012). This suggests that dealumination of the binder is the main mechanism of failure of GPM to acid attack. In contrast to XRD results, gypsum was not found in

GPM sample attacked by H_2SO_4. No further significant changes to the FTIR spectra were observed.

In the case of the PCMs, the main peak was centred at 985 cm^{-1} and shifted to 1039 cm^{-1} after the HCl attack, likely due to decalcification of C-S-H gel formed in PC systems (Bernal *et al.*, 2012). A band at approximately 3640 cm^{-1}, corresponding to O-H stretching vibrations in CH, was not present in samples exposed to the acid attack. Also, a peak at 870 cm^{-1} (out of plane bending of CO_3^{2-}) and a broad band at approximately 1420 cm^{-1} (asymmetric stretching of CO_3^{2-}), both corresponding to $CaCO_3$, were absent from the FTIR spectra of acid attacked samples. A broad shoulder near 1105 cm^{-1}, corresponding to asymmetric stretching vibrations of SO_4^{2-} in ettringite, was no longer present in acid attacked samples. The degraded material after sulphuric acid attack was mainly gypsum, with a very strong signal at 1115 cm^{-1}. Further peaks at approximately 669 (the bending vibration of the SO_4 tetrahedron), 1620, 1685, (both in plane bending vibrations of O-H···O group), 3405 and 3536 cm^{-1} (both the stretching vibrations of O-H···O group) can also be related to the presence of gypsum (Putnis *et al.*, 1990).

5.0 CONCLUSIONS

On the basis of the presented results, the following conclusions have been drawn:

Irrespective of the sulfate solution used (Na_2SO_4 and $MgSO_4$), GPM mix showed superior sulfate resistance when compared with PCM mix. Only small length changes occurred, which are believed to be due to ion exchange between mortar samples and the sulfate solutions. No changes to the geopolymer microstructure were detected. Sulfate attack by both Na_2SO_4 and $MgSO_4$ solutions caused visible deterioration, and large expansion of PCM mix, making it unsuitable for the use in sulfate rich environments. During the course of the test, PCM samples exposed to Na_2SO_4 solutions progressively expanded, which led to their expansive spalling and cracking. Although the expansion of PCM samples exposed to $MgSO_4$ solution was slightly lower than in those immersed in Na_2SO_4, they showed larger surface deterioration. As confirmed by XRD and FTIR results, attack by both sulfate salts caused depletion of calcium hydroxide from the attacked portion of the samples. The presence of expansive salts was detected: gypsum and ettringite for Na_2SO_4 solutions, and gypsum for $MgSO_4$ for solutions. Samples attacked by $MgSO_4$ solution revealed the presence of brucite.

GPM showed better resistance to attack by H_2SO_4 and HCl solutions than PCM, *i.e.* lower surface deterioration and lower mass loss. The rate of mass loss of GPMs decreased, while of PCMs increased, during eight weeks of the acid testing. This suggests that GPM mixes provided a better quality (lower permeability) of acid-degraded layer, which restricted to some extent the diffusion of acid into the microstructure, hence lowering the degree of deterioration. The main mechanism of GPM deterioration was dealumination of the geopolymer microstructure. H_2SO_4 solutions caused higher degree of surface deterioration, mass loss and microstructural changes than corresponding HCl solutions. Where PCMs are concerned, both acids had a dissolution effect on hcp caused by hydrogen ions (primarily dissolution of calcium hydroxide and decalcification of C-S-H and ettringite). In addition, H_2SO_4 acid caused precipitation of gypsum on the samples' surface and within pores of the already degraded near-surface layer, leading to expansive spalling caused by induced tensile stresses.

Sulfate and acid attack on concrete structures is of great concern, in particular for wastewater transport and treatment infrastructure and agricultural applications. The currently used measures to minimise/reduce such deterioration are costly and in many cases require periodic renewal. This work has allowed greater understanding of the performance of a commercial geopolymer binder system in harsh sulfate and acid environments and will assist in the design of alternative concrete solutions. By using these more resistant geopolymer materials, maintenance costs will be reduced and service life increased.

Acknowledgement

The work reported here was a part of Invest Northern Ireland funded collaborative research project (Ref. No.: RDO212970 – Development and commercialisation of banahCEM geopolymer binder) between Queen's University Belfast and banah UK Ltd. The authors are grateful to the Invest Northern Ireland for the financial support and to the School of Natural and Built Environment for provided facilities.

References

Aguiar, J.B., Camões, A., Moreira, P.M., 2008. Coatings for concrete protection against aggressive environments", Journal of Advanced Concrete Technology, 6(1)243-250.

Arellano-Aguilar, R., Burciaga-Díaz, O., Gorokhovsky, A., Escalante-García, J.I., 2014. Geopolymer mortars based on a low grade metakaolin: Effects of the chemical composition, temperature and aggregate:binder ratio. Construction and Building Materials, 50(1)642-648.

ASTM, 2001. Standard test methods for chemical resistance of mortars, grouts, and monolithic surfacings and polymer concretes, ASTM C267-01

ASTM, 2004. Standard test method for length change of hydraulic-cement mortars exposed to a sulfate solution, ASTM C1012/C1012M-04.

Aye, T., Oguchi, C.T., 2011. Resistance of plain and blended cement mortars exposed to severe sulfate attacks, Construction and Building Materials, 25(6) 2988-2996.

Beddoe, R.E., Dorner, H.W., 2005. Modelling acid attack on concrete: Part I. The essential mechanisms, Cement and Concrete Research, 35(12)2333-2339.

Bernal, S.A., Rodríguez, E.D., Mejía de Gutiérrez, R., Provis, J.L., 2012. Performance of alkali-activated slag mortars exposed to acids. Journal of Sustainable Cement-Based Materials, 1(3)138-151.

Bonen, D., Cohen, M.D., 1992. Magnesium sulfate attack on portland cement paste-I. Microstructural analysis, Cement and Concrete Research, 22(1)169-180.

Bouguermouh, K., Bouzidi, N., Mahtout, L., Pérez-Villarejo, L., Martínez-Cartas, M.L., 2017. Effect of acid attack on microstructure and composition of metakaolin-based geopolymers: The role of alkaline activator. Journal of Non-Crystalline Solids, 463(5)128-137.

Burciaga-Díaz, O., Escalante-García, J.I., 2012. Strength and Durability in Acid Media of Alkali Silicate-Activated Metakaolin Geopolymers. Journal of the American Ceramic Society, 95(7)2307-2313.

BSI, 1995, Testing aggregates. Methods for determination of density, BS 812 Part 2.

BSI, 2011. Cement. Composition, specifications and conformity criteria for common cements. BS EN 197 Part 1.

BSI, 2016. Construction Materials. Alkali-activated cementitious material and concrete. Specification. PAS 8820.

Eyles, V.A., 1950. Note on the Interbasaltic Horizon in Northern Ireland. Quarterly Journal of the Geological Society, 106(1)136-137.

Gao, X.X., Michaud, P., Joussein, E., Rossignol, S., 2013. Behavior of metakaolin-based potassium geopolymers in acidic solutions, Journal of Non-Crystalline Solids, 380(11)95-102.

Ghosh, S.N., 1999. IR spectroscopy, In: Handbook of Analytical Techniques in Concrete Science and Technology. Principles, Techniques, and Applications, Eds. Ramachandran, V.S., Beaudoin, J.J., Noyes Publications/William Andrew Publishing, New York, USA, 174-204.

Gutberlet, T, Hilbig, H., Beddoe, R.E., 2015. Acid attack on hydrated cement - Effect of mineral acids on the degradation process, Cement and Concrete Research, 74(8)35-43.

Heath, A., Paine, K., Goodhew, S., Ramage, M., Lawrence, M., 2013. The potential for using geopolymer concrete in the UK. Proceedings of the Institution of Civil Engineers - Construction Materials, 166(4)195-203.

Kwasny, J., Soutsos, M.N., McIntosh, J.A., Cleland, D.J., 2016. banahCEM – comparison of properties of a laterite-based geopolymer with conventional concrete, 9th International Concrete Conference 2016. Environment, Efficiency and Economic Challenges for Concrete, University of Dundee, Scotland, UK, 4–6 Jul 2016, Eds. Jones, M.R. et al. 383–394.

McIntosh, J.A., Kwasny, J., Soutsos, M.N., 2014. Evaluation of Northern Irish Laterites as Precursor Materials for Geopolymer Binders. 34th Cement and Concrete Science Conference, Sheffield, UK, 14–17 Sep 2014, 6 p.

McIntosh, A., Lawther, S.E.M., Kwasny, J., Soutsos, M.N., Cleland, D., Nanukuttan, S., 2015, Selection and characterisation of geological materials for use as geopolymer precursors. Advances in Applied Ceramics, 114(7)378-385.

Mehta, P.K., Monteiro, P.J.M., 2006. Concrete: microstructure, properties, and materials. 3rd ed., McGraw-Hill, New York, USA, 659 pp.

Monteny, J., Vincke, E., Beeldens, A., De Belie, N., Taerwe, L., Van Gemert, D., Verstraete, W., 2000. Chemical, microbiological, and in situ test methods for biogenic sulfuric acid corrosion of concrete, Cement and Concrete Research, 30(4)623-634.

Monteny, J., De Belie, N., Taerwe, L., 2003. Resistance of different types of concrete mixtures to sulfuric acid. Materials and Structures, 36(4)242-249.

Oueslati, O., Duchesne, J., 2012. The effect of SCMs and curing time on resistance of mortars subjected to organic acids. Cement and Concrete Research, 42(1)205-214.

Pacheco-Torgal, F. *et al.*, 2015. Handbook of alkali-activated cements, mortars and concretes, Woodhead Publishing. Eds: Pacheco-Torgal, F. et al., 852 pp.

Putnis, A., Winkler, B., Fernandez-Diaz, L., 1990. In Situ IR Spectroscopic and Thermogravimetric Study of the Dehydration of Gypsum. Mineralogical Magazine, 54(374)123-128.

RILEM TC 211-PAE, 2013. Performance of Cement-Based Materials in Aggressive Aqueous Environments, State-of-the-Art Report. Eds.: Alexander, M., Bertron, A., De Belie, N., 462 pp.

RILEM TC 224-AAM, 2014. Alkali-Activated Materials: State-of-the-Art Report, State-of-the-Art Report. Eds.: Provis, J.L. and van Deventer, J.S.J., 396 pp.

Santhanam, M., Cohen, M.D., Olek, J., 2002. Mechanism of sulfate attack: A fresh look: Part 1: Summary of experimental results. Cement and Concrete Research, 32(6)915-921.